

Converted waves: properties and 3-D survey design

Gijs J.O. Vermeer, 3DSymSam - Geophysical Advice

Summary

The interest in acquiring 3-D/3-C or 4-C seismic data is growing. Several 3-D/3-C surveys have been acquired up till now, but their design has not yet received much attention. This paper considers 3-D/3-C survey design from a theoretical point of view. In the first part properties of PS-waves are investigated in various minimal data sets (3-D single-fold basic subsets of acquisition geometry). The apparent velocities in the 3-D receiver gather are much larger than in the 3-D shot gather. The cross-spread shows significant asymmetry. Illumination, resolution and imaging depend strongly on the minimal data set. In the second part the consequences of these properties for 3-D survey design are reviewed. It turns out that (carefully designed) parallel geometry is a better choice than orthogonal geometry, perhaps even if azimuth-dependent effects need be analyzed. Receiver sampling should be denser than shot sampling.

Introduction

Multi-component surface seismic has a long history on land, but until a few years ago, multi-component marine data acquisition was virtually unheard of. Then, the interest in multi-component marine data acquisition received a great stimulus by the pioneering work of Statoil with their SUMIC technique (Berg et al., 1994; Johansen et al., 1995; Berg and Arntsen, 1996; Granli et al., 1999). Imaging of gas chimneys was the main application of the technique (Berg et al., 1994; Granli et al., 1999). The PS-wave data produced sections suitable for structural interpretation, whereas the P-wave sections only produced jumble across the gas chimneys.

In SUMIC, ROVs were still used to plant the geophones, but now a less expensive technique, based on using a dragged bottom cable, is rapidly being developed. This technique was first tested for 2-D/4-C applications (Kommedal et al., 1997; Kristiansen, 1998). Kristiansen (1998) lists a large number of applications for 4-C (3 geophones plus hydrophone) data.

Full-scale tests of the dragged bottom cable technique for 3-D/4-C surveys have been reported for three different surveys acquired in the North Sea (Kristensen et al., 1999; McHugo et al., 1999; Rosland et al., 1999). The geometries used in these surveys were all different.

In all marine applications, P-wave energy converted to S-wave energy at the reflecting horizons is the main wave type being analysed. These PS-waves have asymmetric raypaths leading to special requirements of the survey geometry. Only a few papers seem to have been published on the design of 3-D/3-C seismic surveys. Lawton (1995), and Cordson and Lawton (1996) deal mostly with binning issues, in association with the asymmetric illumination by PS-waves. In my opinion, binning issues are better left to processing, in particular when spatial interpolation to neighboring bin centers (Herrmann et al., 1997; Beasley and Mobley, 1997) becomes more generally accepted. Recently, Ronen et al. (1999) discussed the irregular illumination by cross-spread 4-C surveys and argued that a careful analysis of this effect is required to plan an optimal survey.

The asymmetric illumination by PS-waves is the major reason that the design of 3-D surveys for converted waves is more complicated than for P- or S-waves. Symmetric sampling requirements (Vermeer, 1998a) do no longer apply. To find out what does apply, this paper looks at some properties of the PS-wavefield in the basic single-fold subsets (minimal data sets, MDSs, see Table 1) of various acquisition geometries. The behavior of apparent velocities in the MDSs is discussed to determine sampling requirements. Illumination, resolution, and imaging of converted waves are compared for the different MDSs. In the second part of the paper, the results of the first part are applied to discuss the suitability of various geometries for PS-wave acquisition. It is found that parallel geometry is most suited for PS-wave acquisition, whereas other geometries tend to have problems with illumination, resolution or both.

The analyses in this paper are carried out for a simple isotropic medium with constant P-wave velocity V_p and constant S-wave velocity V_s .

Designing 3-D/3-C surveys

Table 1 Overview of minimal data sets, their coordinates and geometry

Minimal data set	Shot coordinates	Receiver coordinates	Acquisition geometry
3-D shot	(X, Y)	(x_r, y_r)	Areal
3-D receiver	(x_s, y_s)	(X, Y)	Areal
Cross-spread	(X, y_s)	(x_r, Y)	Orthogonal
Slanted spread	$(X + x_s, Y + \alpha x_s)$	(x_r, Y)	Slanted
COA-gather	(x_s, y_s)	$(x_s + X, y_s + Y)$	Parallel

Properties of the PS-wavefield

Traveltime surfaces and apparent velocity

The difference between V_p and V_s leads to asymmetry between the P- and the S-angles of reflection according to Snell's law. As a consequence, the raypaths are different if shot and receiver are interchanged, and traveltime curves are different in common-shot gathers and common-receiver gathers. For a horizontal reflector, the traveltime curves are still the same, even though the raypaths are different.

Similarly, the diffraction traveltime as a function of offset is different between common-shot diffractions and common-receiver diffractions. In the common shot the diffraction is much steeper because the slow V_s determines the change in traveltime. Figure 1a illustrates the traveltime behavior for PP- and PS-reflections from a horizontal reflector and it shows PP- and PS-diffraction traveltimes for shot and receiver gathers. The corresponding apparent velocities (as measured in the surface coordinate systems) are plotted in Figure 1b. All apparent velocities seem to be controlled by the P-wave velocity only, except the PS-diffraction in the common shot, which has very low apparent velocities tending towards the S-wave velocity.

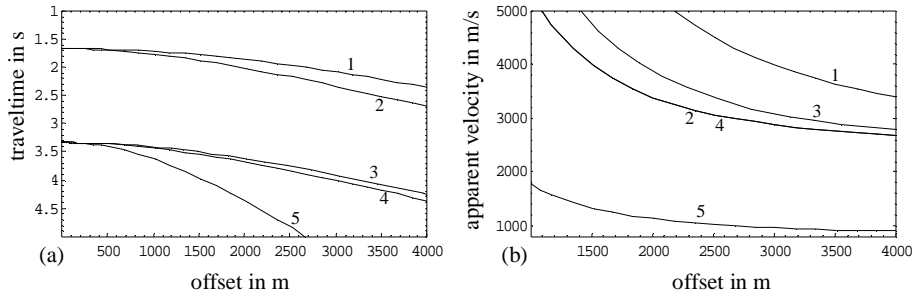


FIG. 1. Traveltime curves (a) and apparent velocity (b) for PP- and PS-reflections and diffractions in constant velocity medium. $V_p = 2400$ m/s, $V_s = 800$ m/s, depth of reflector is 2000 m, diffractor at $(0, 0, 2000)$. 1 = PP-reflection, 2 = PP-diffraction, 3 = PS-reflection, 4 = PS-diffraction in common receiver, 5 = PS-diffraction in common shot.

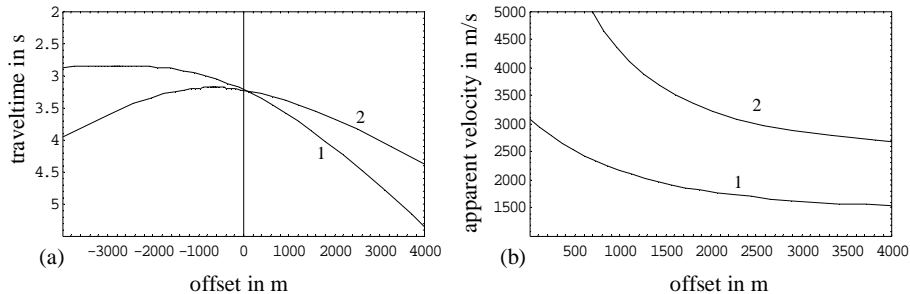


FIG. 2. PS-reflection in common shot (1) and common receiver (2) for 15° dip. Depth of reflector at position of shot, receiver is 2000 m. (a) Traveltimes. (b) Apparent velocity. The common shot has the steepest curve and the smallest apparent velocity.

Designing 3-D/3-C surveys

The asymmetry in PS-acquisition becomes more apparent for dipping reflectors. This is illustrated for a reflector with 15° dip in Figure 2. Note that the reflection time curve is steepest for positive offsets in the common shot; there it has an apparent velocity smaller than the P-wave velocity.

Figure 3 shows contour plots of the diffraction traveltimes for the common receiver, the common shot, the common-offset gather with constant azimuth (COA) and the cross-spread. In the common shot the S-wave velocity determines the slopes of the curves, whereas in the common receiver the P-wave velocity determines the slopes. The curves in the common-offset gather have some intermediate slope. This can be understood by realizing that the apparent velocity V_a in the zero-offset gather would tend to $1/V_a = 1/V_p + 1/V_s$ for large distances from the scatterer. Note that - unlike a PP-diffraction - the apex of the PS-traveltime surface in the COA-gather is offset from the diffractor position. The cross-spread shows a mixed behavior: steep flanks in the in-line (receiver) direction and gentle slopes in the cross-line (source) direction.

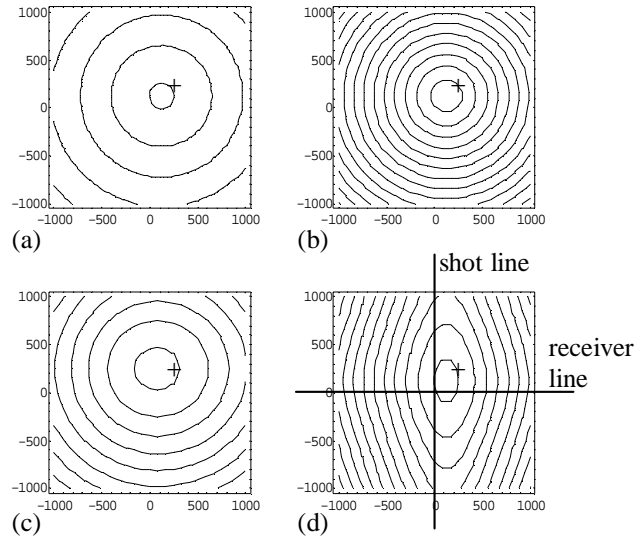


FIG. 3. Diffraction traveltimes for various minimal data sets plotted in midpoint coordinates. Contour interval is 250 ms. Position of diffractor in (250, 250, 500) is indicated by a "+", $V_p = 2400$ m/s, $V_s = 800$ m/s. (a) Common receiver. (b) Common shot. (c) COA gather (600 m). (d) Cross-spread.

Illumination

In P-wave acquisition the midpoint coverage is the same as subsurface coverage of horizontal reflectors. Therefore, fold-of-coverage is fairly representative for illumination fold, even for areas with gentle dips. This is quite different for PS-wave acquisition due to the asymmetry in the raypaths. For three different minimal data sets figure 4 shows a comparison of their midpoint area (the same for all three MDSs) with the illumination areas of a horizontal reflector for $V_p / V_s = 1.5$ and $V_p / V_s = 3$. The midpoint area is the 2000×2000 m square in the figure. It also represents the PP-illumination area for a horizontal reflector. The other curves represent the conversion point curves corresponding to the midpoints along the outline of the square. The cross-spread shows asymmetry: the illumination area is wider in the in-line direction and narrower in the cross-line direction than the midpoint area. The 3-D shot has the largest illumination area and the 3-D receiver the smallest.

For dipping reflectors the illumination areas will shift updip. The illumination area of a COA gather is not shown in Figure 4 to prevent clutter. It would be a square illumination area with the same size as the midpoint area, but shifted towards the receivers.

Often, illumination fold is measured by counting the number of hits per bin. Then, for a binsize equal to the natural binsize of the geometry, illumination fold of a single cross-spread might vary between 0 and 3, whereas there is only a single-fold illumination area. Counting the number of hits per bin neglects the spatial relationship that

Designing 3-D/3-C surveys

exists between groups of traces, such as a cross-spread. Counting the number of overlapping illumination areas gives a better measure of imaging capabilities and image fold (see also Figure 14 and Vermeer, 1998b).

Resolution

The wavenumber spectra of different MDSs can be used to compare the resolution that can be reached with those MDSs (Vermeer, 1999). The spectra are composed from the contributions to the spectrum by all individual shot/receiver pairs. For PP-wavefields, the contribution of each shot/receiver pair to the resolution in a point P is described by (see Figure 5a)

$$\mathbf{k} = \mathbf{k}_s + \mathbf{k}_r = \frac{f}{V_p} (\mathbf{u}_s + \mathbf{u}_r), \quad (1)$$

where \mathbf{k}_s , \mathbf{k}_r are shot, receiver wavenumber respectively, f is frequency, and \mathbf{u}_s and \mathbf{u}_r are unit vectors. For PS-wavefields, a similar relation holds, but now V_s enters the equation as well (see Figure 5b and c):

$$\mathbf{k} = \mathbf{k}_s + \mathbf{k}_r = f \left(\frac{\mathbf{u}_s}{V_p} + \frac{\mathbf{u}_r}{V_s} \right), \quad (2)$$

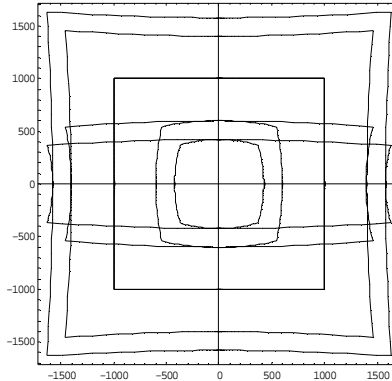


FIG. 4. Illumination of horizontal reflector by 3-D shot (the two widest curves), 3-D receiver (the two curves in the center), and cross-spread (the two elongated curves) for $V_p / V_s = 3$ and $V_p / V_s = 1.5$. The 2000×2000 m square represents the midpoint area of the three minimal data sets. The depth of the reflector is 2000 m.

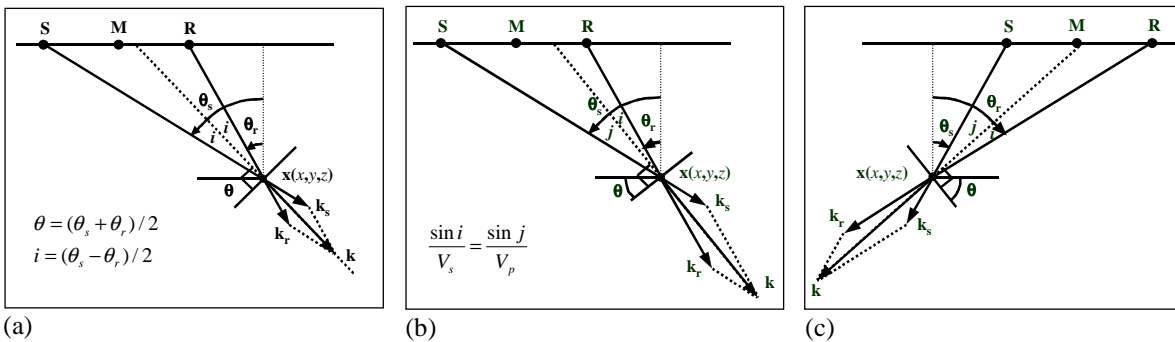


FIG. 5. Illumination of subsurface point \mathbf{x} by single shot/receiver pair (S, R) and corresponding wavenumbers. \mathbf{k}_s and \mathbf{k}_r point in the direction of the raypaths ending in \mathbf{x} . θ is the dip illuminated by (S, R), and i , j are the corresponding reflection angles. (a) PP-situation. (b) PS-situation with R closest to \mathbf{x} . (c) PS-situation with S closest to \mathbf{x} . $V_p/V_s = 2$.

Designing 3-D/3-C surveys

It follows from Eq. 2 that for the PS-wavefield $|\mathbf{k}_r|$ is larger than $|\mathbf{k}_s|$. This leads to asymmetry in illumination and resolution, depending on the relative position of shot and receiver as illustrated in Figure 5b and c. In Figure 5b the vertical component of \mathbf{k} is larger than in Figure 5c, whereas it is the other way around for the horizontal component. Another consequence of Eq. 2 is that - for the same frequency - the components of \mathbf{k} for PS-waves are larger than for PP-waves. The collection of all shot/receiver pairs in an MDS illuminate a wide range of dip angles θ , and span a wide range of wavenumbers, indicative of resolution. For different MDSs, the wavenumber spectra are illustrated in Figure 6 for a PP-wavefield, and in Figure 7 for a PS-wavefield.

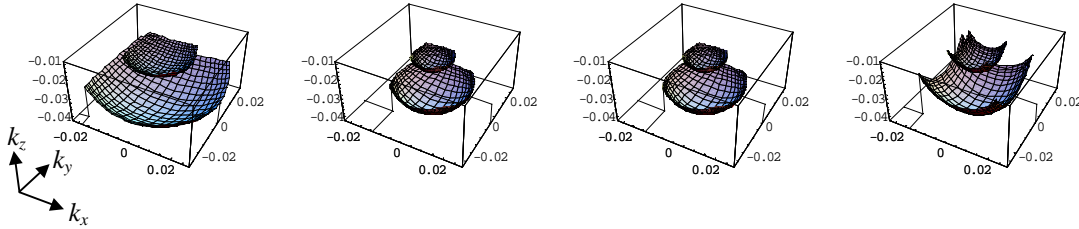


FIG. 6. PP-wavenumber spectra for a subsurface point below the center of each one of four minimal data sets. All data sets have the same 1000×1000 m midpoint area. The surfaces correspond to constant input frequencies 25 Hz (upper surfaces) and 50 Hz. From left to right: 600 m COA gather, 3-D shot, 3-D receiver and cross-spread.

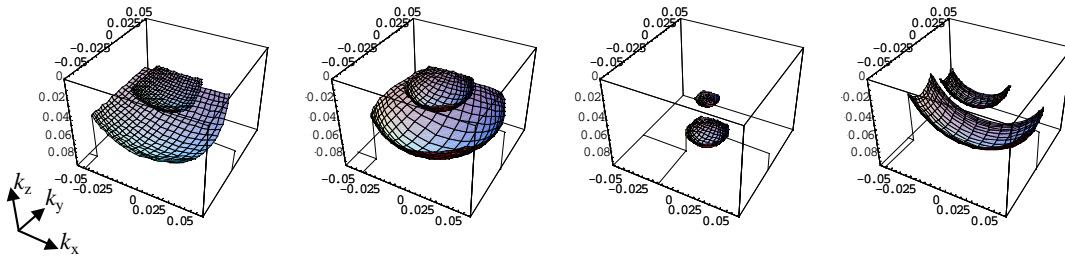


FIG. 7. Same as Figure 6 for PS-situation with $V_p/V_s = 3$. Note that the wavenumber ranges in this figure are larger than in Figure 6; the 3-D receiver spectrum has the same size as in Figure 6.

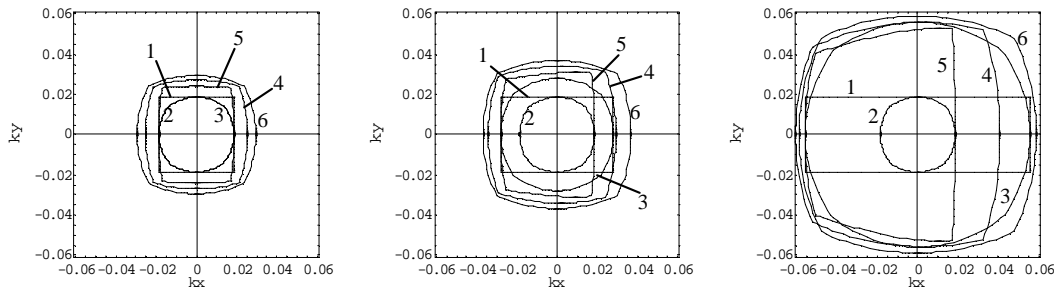


FIG. 8. Projection in horizontal wavenumber plane of the (common-frequency) spectra of six different minimal data sets with the same 1000×1000 m midpoint area for PP (left), PS with $V_s = 1600$ m/s (center) and PS with $V_s = 800$ m/s (right). $V_p = 2400$ m/s in all cases. 1= cross-spread, 2 = 3-D receiver, 3 = 3-D shot, 4 = 600 m COA gather, 5 = 1000 m COA gather, 6 = zero offset. The PS zero-offset is hypothetical, as PS-waves have zero amplitude for zero-offset.

Figure 6 shows that the wavenumber spectra of the 3-D receiver and the 3-D shot are identical for PP-waves, whereas Figure 7 illustrates that the PS-wavenumber spectrum of the 3-D shot spans a much wider range than that of

Designing 3-D/3-C surveys

the 3-D receiver. The cross-spread PS-spectrum has a hammock shape, indicative of the asymmetry between in-line and cross-line direction.

Figure 8 shows the projections on the horizontal plane of wavenumber spectra of various minimal data sets for PP- (left) and PS-waves (center and right). Notable is the invariance of the 3-D receiver resolution to V_p / V_s . This is because V_p is kept constant, whereas the V_p -leg of the raypath fully determines the resolution in the 3-D receiver. The asymmetry in the cross-spread leads to less resolution in the cross-line (source) direction than in the in-line direction. There is also asymmetry in the resolution of the COA gathers. The resolution is best for the downdip shooting part of the wavefield (positive x , y map onto negative k_x , k_y , hence a shot-receiver combination with positive coordinates, source to the left of the receiver, maps to negative k).

Figure 8 shows that - except for the 3-D receiver gather - the resolution of PS-data is better than the resolution of PP-data *for the same frequency* and the same aperture (midpoint range). In practice, PS-data tend to have lower maximum frequency than PP-data, thus reducing or even losing the relative advantage.

Imaging

Next to the range of wavenumbers that is available for the imaging process, it is of interest to investigate the imaging process itself, and compare the ability of various MDSs for imaging of the PS-wavefield. For this investigation, it is helpful to consider migration as a two-step process (see Figure 9), similar to the discussion of the effect of sampling density on the migration result in Vermeer (1999).

In the first step, reflections are turned into bowl-shaped events, with the apex at the point of stationary phase. In the second step, all data of the migration panel are summed and provide the image trace. Similar as for forward modeling (Brühl et al., 1996), the zone of influence can be defined. The zone of influence encompasses all traces around the point of stationary phase, which contribute —constructively or destructively— to the amplitude of the migrated event at the depth of the image point. The width of the zone of influence (sometimes called Fresnel zone) depends on the length of the wavelet, on the curvature of the migration-corrected event, and on the domain in which the zone is measured, midpoint domain or subsurface domain (see below). The data outside the zone of influence cannot contribute to the required image and should be canceled in the second step of the migration process.

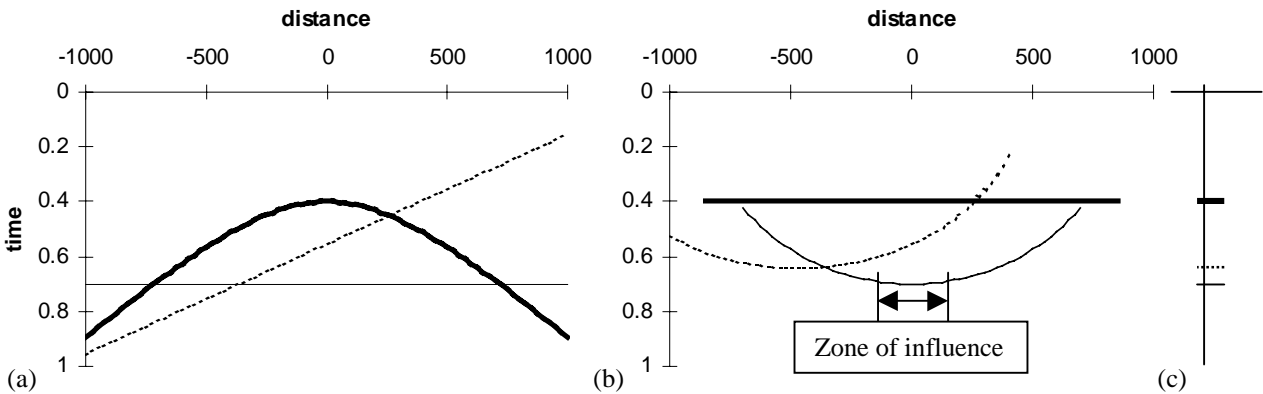


FIG. 9. Migration as a two-step process illustrated with a zero-offset section. (a) Input showing diffraction (heavy curve), a dipping reflection (thin dotted curve), and a horizontal reflection (thin drawn curve). (b) Migration panel. In the first step, the input data are realigned according to the diffraction traveltimes in the output point. Shown is the realignment for the output point at $x = 0$, which is the position of the diffractor. Note that the apex of the curve for the horizontal event is located at $x = 0$, whereas the apex for the dipping event is located toward the left. The location of these apices corresponds to the position of the zero-offset shot/receiver pair, which has illuminated the reflector at $x = 0$. (c) In the second step, the realigned data are summed (stacked) and phase-corrected to form the image trace.

Designing 3-D/3-C surveys

In 3-D, the migration-corrected reflections become truly bowl-shaped events. To describe the shape of these events in 3-D, contour plots are used in Figures 10 and 11. Figure 10 shows for P-wave data that the zone of influence is not very different between the various MDSs. (If the output point does not coincide with the center of the minimal data set, the differences become larger.) Figure 11 shows for PS-data that large differences exist between the various MDSs.

For proper imaging, it is essential to have complete zones of influence in the migration summation. The elongated shape of the zone of influence in the cross-spread requires more traces in the cross-line direction than in the in-line direction. This suggests acquisition of asymmetric cross-spreads with much longer shotlines than receiver lines, and it suggests that an asymmetric migration operator range should be used.

The zone of influence contains more data points (traces) in the cross-spread than in the 3-D shot. This would lead to a larger amplitude for cross-spread data than for 3-D shot data. True-amplitude migration should take these effects into account.

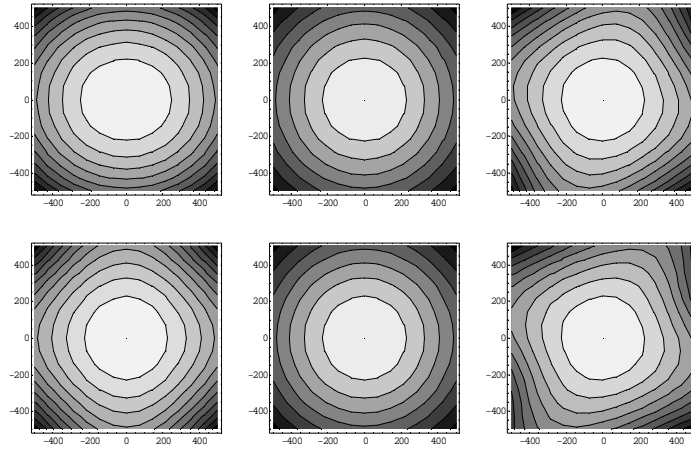


FIG. 10. Contour maps in (x_m, y_m) of migration-corrected PP-traveltimes of horizontal reflector for output point in center of six different MDSs. Top row: COA-gather, 3-D receiver, and slanted spread. Bottom row: Cross-spread, 3-D shot, and zigspread. The central (white) area in each map may be considered to represent the zone of influence. Depth of reflector 1000 m. $V_p = 2400$ m/s. Contour interval 25 m.

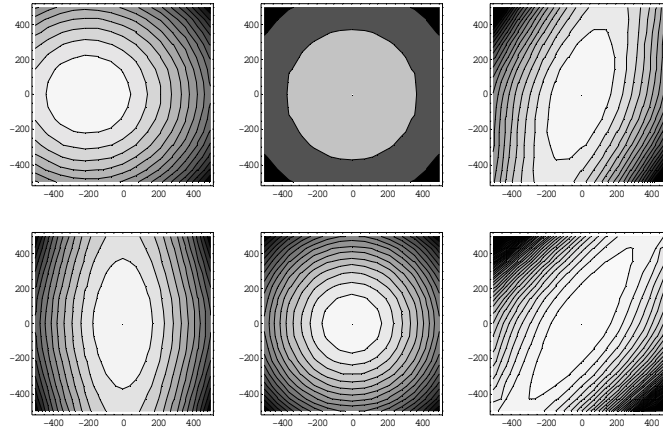


FIG. 11. As Figure 10 for PS-reflection with $V_p/V_s = 2$. The zones of influence are very different for the different MDSs. These zones give a representation of the *number* of reflection points being "stacked" into the output point.

Designing 3-D/3-C surveys

In Figure 12 the zones of influence are plotted as a function of reflection point x and y , rather than in terms of midpoint x and y as in Figure 11. Figure 12 shows that the subsurface area contributing to the migration amplitude in the output point is about the same in all cases. There are small differences, depending on the offset mix contributing to the area of the zone of influence. Larger differences would occur if the output point would not coincide with the center of the MDSs.

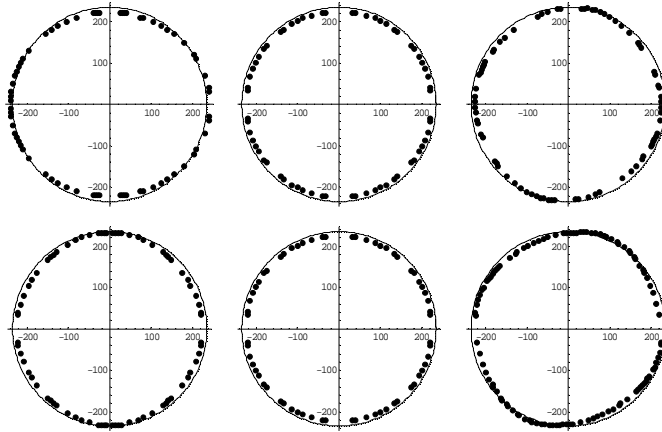


FIG. 12. Central contour at 975 m of Figure 11 replotted as function of reflection point x and y (dots). The drawn circle with the same radius in all plots has been added as a reference. These curves give a better representation of the *range* of reflection points being "stacked" into the output point than the curves in Figure 11. (The contours are plotted as a series of dots rather than as drawn lines, because of difficulty to compute contours; each dot represents a point in a narrow range around 975 m.)

3-D survey design for PS-waves

Choice of geometry

Very often the choice of geometry will be dictated by circumstances such as available budget. On land, this tends to lead to orthogonal geometry or some derivative thereof (e.g. slanted shotlines), for marine streamer acquisition to parallel geometry and for OBC work to orthogonal geometry. Nevertheless, geophysical requirements should play a role as well, and need to be properly understood. In the first part of this paper we have seen that illumination depends strongly on which minimal data set is used, hence on acquisition geometry. For equal aperture, resolution between the various MDSs is also very different. In this part I discuss the consequences of the properties of the PS-waves in the various MDSs for 3-D/3-C survey design.

There is a large difference in the properties of parallel geometry as compared to the properties of all other geometries. In its ideal form, the parallel geometry is a *translational* geometry, i.e., its properties do not depend on location, whereas all other geometries are non-translational, i.e., their properties vary from point-to-point. This difference manifests itself most clearly in the MDSs. The COA-gather extends across the whole survey area, whereas the MDSs of all other geometries have limited extent, because the shot/receiver offset increases away from the center of those minimal data sets until being cut off.

Orthogonal geometry

For P-wave acquisition and processing, the problem of MDSs of limited extent can be solved quite reasonably by the introduction of pseudo-minimal data sets (pMDS, Vermeer, 1998b). For a regular orthogonal geometry, pMDSs can be constructed as follows: each cross-spread is split into as many small rectangles as the fold-of-coverage, with the number of rectangles in the cross-line direction equal to the cross-line fold, and the number of rectangles in the in-line direction equal to the in-line fold (see Figure 13). Taking together all rectangles with the same relative

Designing 3-D/3-C surveys

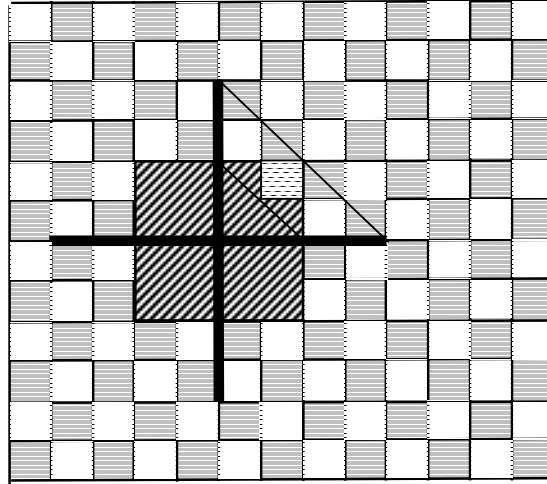


FIG. 13. Tiling of orthogonal geometry with offset/azimuth slots. Each slot has the size of a unit cell. In this case a single-fold tiling composed of upper right corners of all cross-spreads is indicated. The cross-spread is drawn to illustrate the construction of each slot. The upper right corner consists of all midpoints corresponding to the shots and the receivers between the endpoints of the drawn diagonal lines. In this example 16 different slots can be extracted from each cross-spread.

position in each cross-spread provides a single-fold tiling of the whole survey area (these pMDSs are called common-offset-vector gathers in Cary, 1999). The number of different tilings equals the total fold. Between the rectangles (tiles) in each tiling spatial discontinuities exist, but these discontinuities tend to be of limited significance. If the illumination of a reflector in the subsurface is considered, the illumination by adjacent tiles in a tiling will be nearly continuous (depending on the size of the tiles, and the curvature of the reflector), with small overlaps and small gaps. This approach tends to work for P-wave data because the illumination area of each cross-spread is about equal in size to the midpoint area of the cross-spread; these areas have exactly the same size when a horizontal reflector in a constant-velocity medium is illuminated.

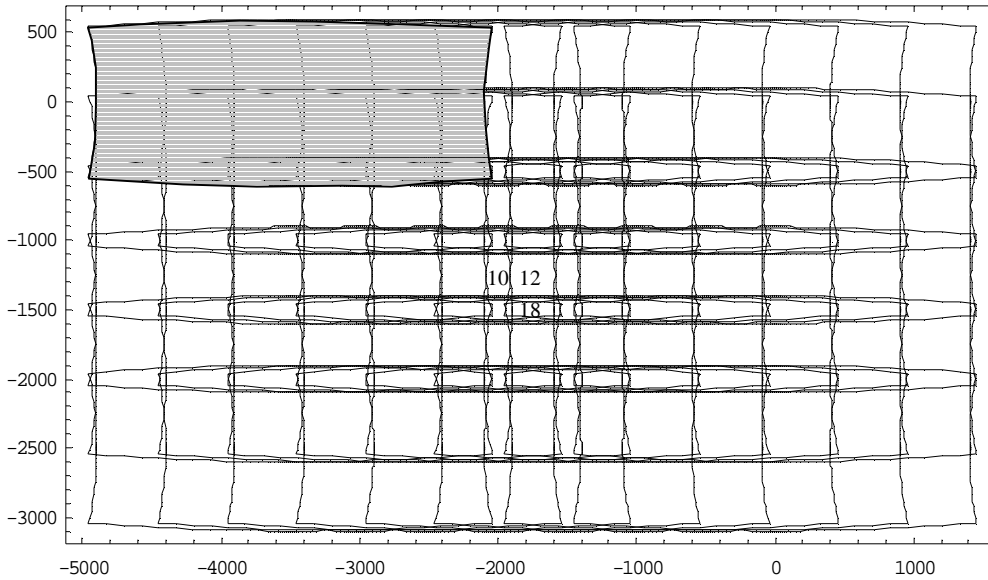


FIG. 14. Overlapping illumination areas for 16-fold orthogonal geometry. $V_p/V_s = 2$. Grey area indicates illumination area of one cross-spread. In narrow horizontal strip PS-illumination fold varies between 15 and 18, whereas in broader horizontal strip illumination fold varies between 10 and 12.

Designing 3-D/3-C surveys

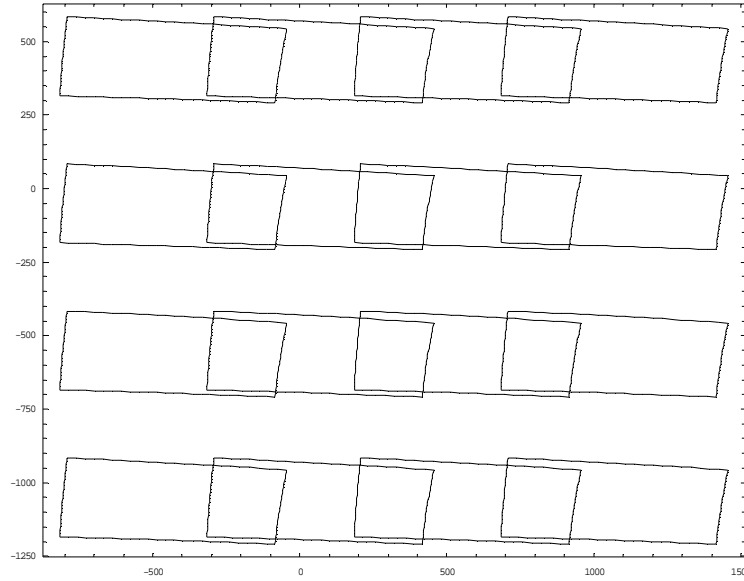


FIG. 15. PS-illumination of horizontal reflector by single-fold tiling of offset/azimuth slots for $V_p/V_s = 2$. The offset/azimuth slots correspond to the upper right-hand corners of 16 cross-spreads as described in Figure 13. Even though fold-of-coverage is exactly one throughout, illumination fold varies between 0 and 2.

These considerations do not apply to PS-wave acquisition and processing. Now the illumination area of each cross-spread is very different from the midpoint area, even for a horizontal reflector in a constant-velocity medium (see Figure 4). As a consequence, regular fold-of-coverage does not lead to regular illumination fold. Figure 14 illustrates the variation of illumination fold for a 16-fold square orthogonal geometry and $V_p/V_s = 2$. For larger V_p/V_s , the variation in illumination fold would be even larger. It is still possible to construct single-fold tilings across the whole survey area by taking rectangles from the same location in each cross-spread, but their illumination areas are strongly discontinuous (Figure 15). Similar reasoning applies to all other non-translational geometries.

As a consequence, it is impossible to obtain a regular PS-illumination of the subsurface using one of the non-translational geometries. The problem is mitigated by using a high fold-of-coverage, and may be reduced further by careful processing.

In orthogonal geometry, resolution in the receiver line direction is determined by the S-wave velocity and in the shot line direction by the P-wave velocity. Therefore, as shown in Figure 6-8, resolution is much better in the receiver line direction than in the shot line direction. In case of a dominant dip direction, it is advisable to orient the receiver lines in that direction.

Parallel geometry

The ideal parallel geometry consists of a collection of pure COA-gathers in which each COA-gather has indeed constant offset and constant azimuth. The ideal geometry can only be acquired by acquisition of each midpoint line separately (repeated 2-D). Acquiring the seismic data in this way is highly expensive; therefore, parallel geometry is always acquired with a number of shot and receiver lines in one pass. In streamer acquisition, the configuration often consists of two shotlines (produced by two source arrays towed behind the vessel) and 4 to 12 streamers. In this way 8 to 24 midpoint lines are acquired in one boat pass.

Because laying cables is time-consuming and shooting sources is relatively cheap, OBC acquisition tends to be carried out the other way around: there the configuration (a swath) is formed by a few receiver lines (often two cables) and many shot lines. Figure 16 shows an arrangement in which the cables are laid out at a distance of 210 m from each other. If the next two cables are shifted over 420 m, the total width covered by the shot lines must be 840

Designing 3-D/3-C surveys

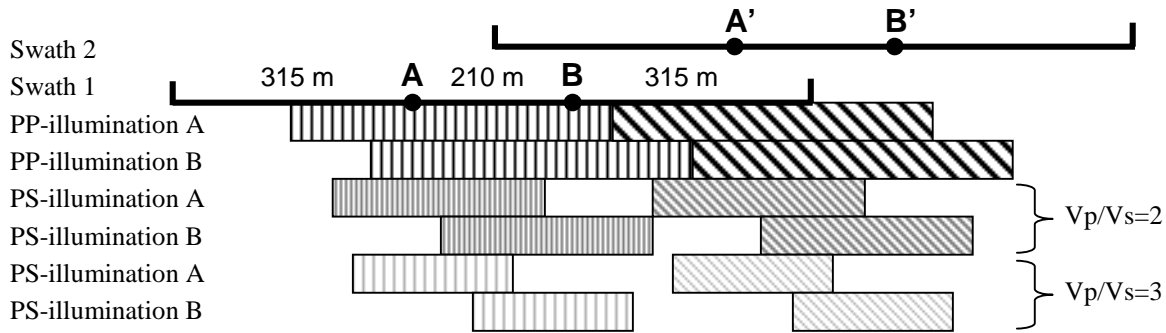


FIG. 16. Illumination with swath acquisition. In swath 1 two cables A and B are laid out at the sea bottom at 210 m distance. The range of shotlines equals 840 m. Swath 2 is shifted over 420 m with respect to swath 1. Illumination of a horizontal reflector for swath 1 is indicated with vertical shading, for swath 2 with diagonal shading. This geometry ensures regular midpoint coverage, i.e., regular PP-illumination of a horizontal reflector. PS-illumination is not regular and even shows gaps in case of large V_p/V_s .

m in order to produce regular midpoint coverage in the cross-line direction. This leads to 315 m width of shot lines outside each cable.

The geometry of the swath was selected such that the midpoint lines of one cable can be interleaved with those of the other cable. In our example, setting the origin halfway the two cables, the cables are at locations ± 105 m, and the shotlines should be at ± 30 m, ± 90 m, etc, until ± 390 m, assuming 60 m shotline interval. This leads to $840/60 = 14$ shotlines and $14 \times 2 = 28$ midpoint lines with $420/28 = 15$ m cross-line interval. In this way cross-line fold is always one, and the total fold only depends on the in-line parameters. (Note that the arithmetic requires setting the width of the geometry at 840 m, which is number of shotlines times shotline interval, rather than taking the distance between the two outside shotlines which is 780 m.)

Figure 16 illustrates that PS-illumination with this acquisition geometry is no longer regular, because the illumination ranges for each cable are narrower than the 420 m midpoint range. For large V_p/V_s values, there are even illumination gaps. The gaps are largest for large in-line offsets (as can be understood by inspection of the illumination area of a cross-spread as shown in Figure 4). For the situation of Figure 16 ($V_p/V_s = 3$, depth of reflector is 2000 m), the illumination gap equals ≈ 53 m. Hence, by adding only a few shotlines on either side of the swath, complete illumination can be achieved. Yet, the remaining density variation in illumination will lead to amplitude striping, unless very careful processing is carried out.

Areal geometry

The areal geometry is also a non-translational geometry. It is the geometry used in the Teal South timelapse experiment (Ridyard et al., 1998). The use of areal geometry tends to be practical only with 3-D receiver gathers and not with 3-D shot gathers. Unfortunately, the illumination area of a 3-D receiver is relatively small, whereas resolution tends to be lower than achievable with PP-data. This requires a relatively high density of 4-C receivers. An advantage of this geometry is that it is most suitable for analysis of azimuth-dependent effects.

Figure 17 illustrates the illumination fold of a 16-fold areal geometry for $V_p/V_s = 2$. The geometry is equivalent to the orthogonal geometry used to produce Figure 14, i.e., the distance between receiver units in x and y is equal to the acquisition line intervals of the orthogonal geometry, and the maximum in-line and cross-line offsets are also equal to those of the orthogonal geometry. Illumination fold varies between 4 and 9 and fold would be even smaller for larger V_p/V_s . The distance between the receiver units would have to be reduced considerably to reach illumination folds of 16 on average.

Figure 18 illustrates the illumination by the top-right corner of each common-receiver gather for the geometry illustrated in Figure 17. Similar as in Figure 15, the midpoints of this data set form a continuous coverage of the survey area. Figure 18 shows that illumination is far from continuous.

Designing 3-D/3-C surveys

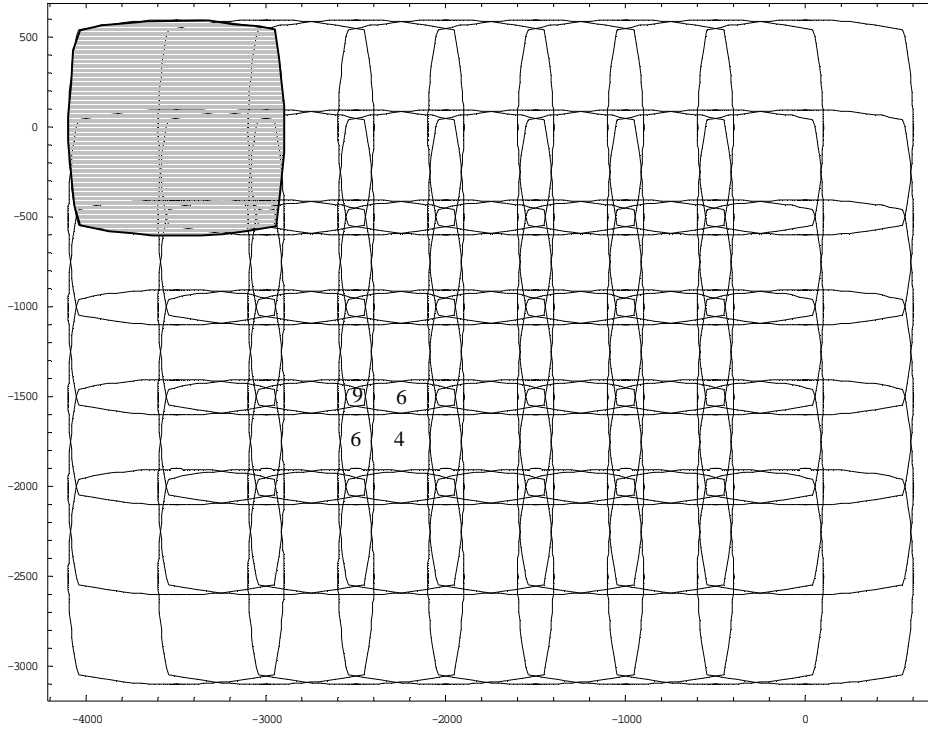


FIG. 17. Overlapping illumination areas for 16-fold areal geometry. $V_p/V_s = 2$. Grey area indicates illumination area of one common receiver. In narrow horizontal strip PS-illumination fold varies between 6 and 9, whereas in broader horizontal strip illumination fold varies between 4 and 6.

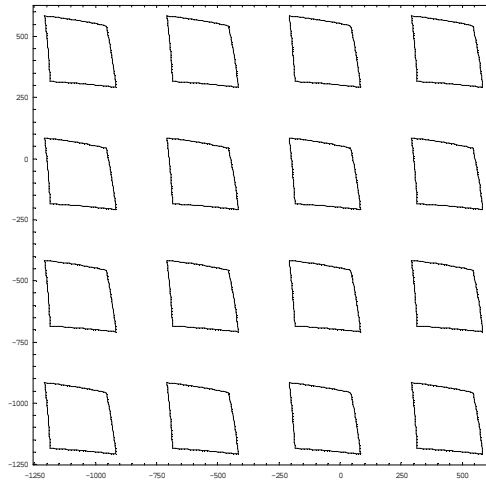


FIG. 18. PS-illumination of horizontal reflector by single-fold tiling of offset/azimuth slots for $V_p/V_s = 2$. The offset/azimuth slots correspond to the upper right-hand corners of 16 common-receiver gathers similar as described for cross-spread geometry in Figure 13. Even though fold-of-coverage is exactly one throughout, illumination fold varies between 0 and 1.

Designing 3-D/3-C surveys

Parallel versus orthogonal geometry and areal geometry

Illumination appears to be the most important property determining which geometry is to be preferred for PS-acquisition. Irregular illumination cannot be avoided by either parallel (except repeated 2-D) or orthogonal geometry. Yet, it appears that taking the irregularity into account in processing is easier with parallel geometry than with orthogonal geometry. The reason is that in parallel geometry common in-line offset gathers are continuous in the in-line direction and can be made to have some overlapping illumination in the cross-line direction. Hence, it can be attempted to regularize the illumination areas of each common-in-line-offset gather by removing overlaps (interpolation might be more difficult). In orthogonal geometry or areal geometry it does not seem to be possible to create (continuous) single-fold illumination gathers from the data.

For resolution, parallel geometry is to be preferred over orthogonal and areal geometry as well. In parallel geometry, horizontal resolution is better for downdip than for updip shooting, whereas vertical resolution is better for updip than for downdip shooting (cf. Figure 5b and c). This problem can be taken care of by center-spread acquisition. On the other hand, in orthogonal geometry, resolution of cross-line dips is inferior to in-line dips. This problem might be alleviated by using an asymmetric migration operator radius, with a considerably larger radius in the cross-line direction than in the in-line direction. However, resolution is also affected by the large spatial discontinuities between the illumination areas of separate cross-spreads. These lead to migration artefacts.

Hence, parallel geometry tends to be better geometry for PS-acquisition than orthogonal or any other crossed-array geometry. Apart from a cost benefit, the only advantage of orthogonal geometry is that it allows analysis of azimuth-dependent effects such as fracture orientation. This would require two orthogonal acquisition passes with parallel geometry. However, if anisotropy is only a nuisance, making life of the processor difficult, then parallel geometry suffers least from its presence. An advantage of areal geometry over orthogonal geometry might be that the irregularities in areal geometry are symmetric, including more symmetry in azimuth-dependent effects.

Sampling

The sampling interval in any spatial domain is determined by the smallest apparent velocity and the largest frequency. This means that for equal maximum frequency the sampling of the receivers in a common shot depends on the S-wave velocity requiring denser sampling than for P-wave acquisition, whereas the sampling of the shots in a common receiver can be the same as for P-wave acquisition. This leads to asymmetric sampling requirements.

Sampling parallel geometry is of special interest. Here again, proper sampling of the field data requires a smaller sampling interval for the receivers than for the shots. The required midpoint sampling of the COA-gather (see Figure 3) depends on the harmonic average of P-wave and S-wave velocities, hence seems to be less strict than in the 3-D-shot gather. However, to realize the required midpoint sampling for each offset, shot and receiver sampling intervals would have to be equal to the required midpoint sampling interval, because each offset only occurs at every other midpoint. Therefore, proper sampling of COA-gathers can best be achieved by interpolation of properly sampled shot and receiver gathers.

Areal geometry can be sampled more efficiently using a hexagonal sampling grid, both for the receiver units and the shotpoints (Vermeer, 1997).

Discussion

In this paper some theoretical considerations have been given on the design of 3-D/3-C seismic surveys. A very simple model was used. It will be interesting to see whether these theoretical considerations can be confirmed by analysis of the 3-D/3-C surveys acquired up till now.

Chevron's Alba survey was acquired with parallel geometry (McHugo et al., 1999). The cross-line midpoint range of their geometry was 1050 m (42 source lines times 50 m interval / 2), for a cross-line shift between swaths of 800 m, giving a 250 m midpoint overlap between adjacent swaths. This geometry ensures full PS-illumination in the cross-line direction of horizontal reflectors for V_p/V_s ratios up to 3. Illumination-density variations in the cross-line direction are inevitable and need be addressed in processing. The geometry has large cross-line offsets, leading to gaps in the shallow illumination. The authors report that "the converted wave processing gave an excellent image of the target zone".

Designing 3-D/3-C surveys

Amoco's Valhall survey was acquired with orthogonal geometry (Rosland et al., 1999). One reason to use orthogonal geometry was that 2-D tests in the area showed weak but non-negligible cross-line energy, possibly caused by azimuthal anisotropy (Thomsen et al., 1997). However, the 3-D processing results reported up till now were obtained without exploiting this cross-line energy (Brzostowski et al., 1999).

Statoil's Statfjord survey was acquired with a very dense coverage of shots across 8 4-C cables of 5 km each and 300 m between the cables (Kristensen et al., 1999). This survey lends itself to simulation of orthogonal geometry and areal geometry. Parallel geometry might also be simulated.

For all these data sets the authors are encouraged by results obtained thus far, but acknowledge that more work needs to be done to fully exploit the vector-information contained in the data and to assess the potential of these methods. I expect that further work will also provide confirmation of predictions based on this theoretical work.

Conclusions

Designing 3-D surveys for PS-waves needs to take the asymmetric raypath and illumination into account. Orthogonal geometry leads inevitably to irregular illumination, which requires special attention in processing, whereas carefully designed parallel geometry may achieve an illumination which approaches the regularity for P-wave acquisition. On the other hand, parallel geometry is not suitable for analysis of azimuth-dependent effects, unless two acquisition passes are carried out. At the end of the day, the sampling requirements of both P-wave and PS-wave acquisition have to be harmonized, taking into account differences in maximum frequency between the two wave types.

Acknowledgment

Kees Hornman is thanked for his critical review of this paper.

References

- Beasley, C.J., and Mobley, E., 1997, Spatial dealiasing of 3-D DMO: 67th Ann. Internat. Mtg., Soc. Expl. Geophys., Expanded Abstracts, paper SP3.7
- Berg, E., Svenning, B., and Martin, J., 1994, SUMIC: Multi-component sea-bottom seismic surveying in the North Sea – data interpretation and applications: 64th Ann. Internat. Mtg., Soc. Explor. Geophys., Expanded Abstracts, 477-480.
- Berg, E., and Arntsen, B., 1996, The potential of subsea seismic: paper EAGE Workshop on Advances in Multi-Component Technology.
- Brühl, M., Vermeer, G.J.O., and Kiehn, M., 1996, Fresnel zones for broadband data: *Geophysics*, **61**, 600-604.
- Brzostowski, M., et al., 1999, 3D converted-wave processing over the Valhall field: 61st Mtg., Eur. Assoc. Geosc. and Eng., Extended Abstracts, paper 6-43.
- Cary, P., 1999, Common-offset-vector gathers: an alternative to cross-spreads for wide-azimuth 3-D surveys: 69th Ann. Internat. Mtg., Soc. Expl. Geophys., Expanded Abstracts, paper xx.
- Cordsen, A., and Lawton, D.C., 1996, Designing 3-component 3-D seismic surveys: 66th Ann. Internat. Mtg., Soc. Expl. Geophys., Expanded Abstracts, paper Acq3.7.
- Granli, J.R., Arntsen, B., Sollid, A., and Hilde, E., 1999, Imaging through gas-filled sediments using marine shear-wave data: *Geophysics*, **64**, 668-677.
- Herrmann, P., David, B., and Suaudeau, E., 1997, DMO weighting and interpolation: EAGE Extended Abstracts, Volume 1, paper A050.
- Johansen, B., Holberg, O., and Øvrebø, O.K., 1995, Sub-sea seismic: impact on exploration and production: 27th Annual OTC, paper OTC 7657.
- Kommedal, J.H., Barkved, O.I., and Thomsen, L.A., 1997, Acquisition of 4 component OBS data - a case study from the Valhall field: 59th Mtg., Eur. Assoc. Geosc. and Eng., Extended Abstracts, paper B047.
- Kristensen, Å., et al., 1999, A 3D/4C OBC survey at the Statfjord field: 61st Mtg., Eur. Assoc. Geosc. and Eng., Extended Abstracts, paper 6-41.

Designing 3-D/3-C surveys

- Kristiansen, P., 1998, Application of marine 4C data to the solution of reservoir characterisation problems: 68th Ann. Internat. Mtg., Soc. Explor. Geophys., Expanded Abstracts, 908-909.
- Lawton, D., 1995, Converted-wave 3-D surveys: design strategies and pitfalls: Can. Soc. Expl. Geophys., Ann. Mtg. Abstracts, 69-70.
- McHugo, S., et al., 1999, Acquisition and processing of 3D multicomponent seabed data from Alba field - a case study from the North Sea: 61st Mtg., Eur. Assoc. Geosc. and Eng., Extended Abstracts, paper 6-26.
- Ridyard, D., Maxwell, P., Fisseler, G., and Roche, S., 1998, A novel approach to cost effective 4C/4D - the Teal South experiment: EAGE Extended Abstracts, Volume 1, paper 2-01.
- Ronen, S., Bagaini, C., Bale, R., Caprioli, P., and Keggins, J., 1999, Coverage and illumination of sea bed 4C surveys: 61st Mtg., Eur. Assoc. Geosc. and Eng., Extended Abstracts, paper 6-18.
- Rosland, B., Tree, E.L., and Kristiansen, P., 1999, Acquisition of 3D/4C OBS data at Valhall: 61st Mtg., Eur. Assoc. Geosc. and Eng., Extended Abstracts, paper 6-17.
- Thomsen, L.A., Barkved, O.I., Haggard, B., Kommedal, J.H., and Rosland, B., 1997, Converted-wave imaging of Valhall reservoir: 59th Mtg., Eur. Assoc. Geosc. and Eng., Extended Abstracts, paper B048.
- Vermeer, G.J.O., 1997, Streamers versus stationary receivers: Proc. Offshore Tech. Conf., paper OTC8314, 331-346.
- Vermeer, G.J.O., 1998a, 3-D symmetric sampling: Geophysics, **63**, 1629-1647.
- Vermeer, G.J.O., 1998b, Creating image gathers in the absence of proper common-offset gathers: Exploration Geophysics, **29**, 636-642.
- Vermeer, G.J.O., 1999, Factors affecting spatial resolution: Geophysics, **64**, 942-953.